iScience

CellPress
OPEN ACCESS

Article

Altered inhibitory function in hippocampal CA2 contributes in social memory deficits in Alzheimer's mouse model

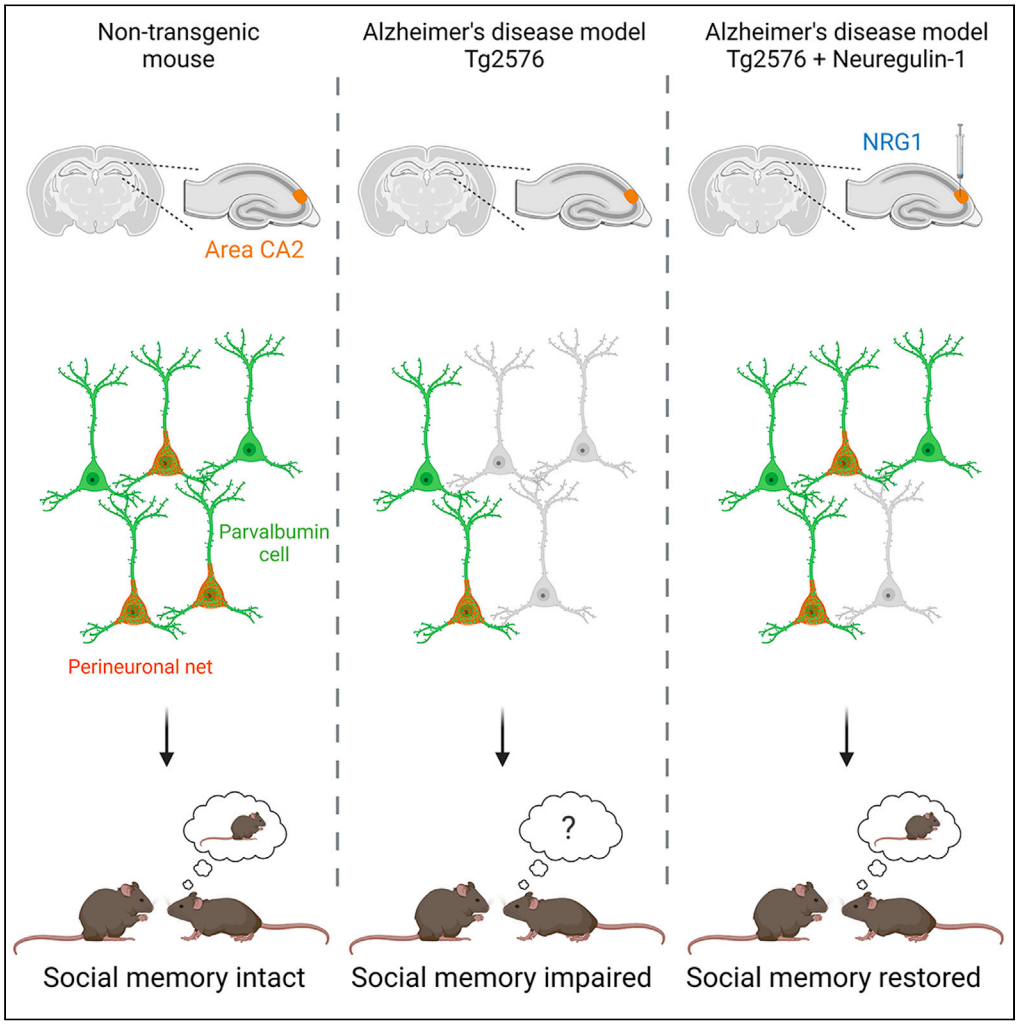

Christophe Clément Rey, Vincent Robert, Guillaume Bouisset, ..., Claire Rampon, Vivien Chevaleyre, Laure Verret

laure.verret@univ-tlse3.fr

Highlights

Tg2576 mouse model of AD have normal sociability, but cannot form social memory

Tg2576 mice have less detectable PV interneurons and PNN in hippocampal area CA2

PV-dependent long-term plasticity is altered in CA2 of Tg2576 mice

NRG1 in CA2 increases PV/PNN and restores social memory of these AD mice

Rey et al., iScience 25, 103895
March 18, 2022
https://doi.org/10.1016/j.isci.2022.103895

iScience

CellPress
OPEN ACCESS

Article

Altered inhibitory function in hippocampal CA2 contributes in social memory deficits in Alzheimer's mouse model

Christophe Clément Rey,[1] Vincent Robert,[2,4] Guillaume Bouisset,[1] Maïthé Loisy,[2] Sébastien Lopez,[1] Vanessa Cattaud,[1,5] Camille Lejards,[1] Rebecca Ann Piskorowski,[2,3,5] Claire Rampon,[1] Vivien Chevaleyre,[2,3,5] and Laure Verret[1,6,*]

SUMMARY

Parvalbumin (PV)-expressing interneurons which are often associated with the specific extracellular matrix perineuronal net (PNN) play a critical role in the alteration of brain activity and memory performance in Alzheimer's disease (AD). The integrity of these neurons is crucial for normal functioning of the hippocampal subfield CA2, and hence, social memory formation. Here, we find that social memory deficits of mouse models of AD are associated with decreased presence of PNN around PV cells and long-term synaptic plasticity in area CA2. Furthermore, single local injection of the growth factor neuregulin-1 (NRG1) is sufficient to restore both PV/PNN levels and social memory performance of these mice. Thus, the PV/PNN disruption in area CA2 could play a causal role in social memory deficits of AD mice, and activating PV cell pro-maturation pathways may be sufficient to restore social memory.

INTRODUCTION

Alzheimer's disease (AD) is characterized by inexorable loss of memory and other cognitive functions. Among the cognitive impairments observed in AD patients, one of the most excruciating is their inability to recognize or remember others. This dysfunction of social memory in AD places an enormous burden on patients, their families, and society, illustrating how much this cognitive function is necessary for appropriate behavioral responses to social interactions. Albeit essential, little is known about the mechanisms responsible for social memory and social recognition deficits in AD.

Long-neglected in studies of hippocampal learning and memory processes, area CA2 has aroused renewed interest because the demonstration of its crucial role in social memory and recognition. Indeed, specific lesioning or genetically-targeted silencing of area CA2 induces social memory deficits without affecting performance in other types of hippocampal-dependent memory (Hitti and Siegelbaum, 2014; Stevenson and Caldwell, 2014). Compared to the CA1 and CA3 hippocampal subfields, area CA2 has atypical anatomical and functional characteristics, including a high density of parvalbumin (PV)-expressing interneurons as well as the perineuronal net (PNN), a specialized extracellular matrix (Botcher et al., 2014; Carstens et al., 2016; Celio, 1993). These PV interneurons are known to exert feedforward inhibition onto area CA2 pyramidal neurons, very tightly regulating CA2 action potential firing (Nasrallah et al., 2019). Moreover, PV cells in area CA2 express a unique form of plasticity in the hippocampus: they undergo a long-term depression of GABA release (iLTD) (Piskorowski and Chevaleyre, 2013), that results in disinhibition of CA2 pyramidal cells (Nasrallah et al., 2015). Hence, iLTD in area CA2 depends on the presence and the activity of PV cells (Nasrallah et al., 2019), and is directly involved in social memory performance (Domínguez et al., 2019; Leroy et al., 2017).

Our previous work has demonstrated that PV cell dysfunction is linked to aberrant brain activity and cognitive deficits in AD mouse models (Verret et al., 2012). We also described that earliest and most significant decrease in PV cells and PNN in the hippocampus of Tg2576 mouse model of AD occurs in the CA2 pyramidal layer (Cattaud et al., 2018), suggesting that both the plasticity of local PV interneuron plasticity as well as associated memory functions may be disrupted in this AD mouse model. The presence of PNN around PV cells is crucial for normal CA2 function, as it is required for the emergence of iLTD at PV interneuron

[1]Centre de Recherches sur La Cognition Animale, Centre de Biologie Intégrative, Université de Toulouse, CNRS, UPS, 31062 Toulouse, France

[2]University of Paris, Inserm UMR_S1266, Institute of Psychiatry and Neuroscience of Paris. Team Synaptic Plasticity and Neural Networks, 102-108 Rue de La Santé, 75014 Paris, France

[3]GHU PARIS Psychiatrie & Neurosciences, 75014 Paris, France

[4]Present address: New York University Neuroscience Institute, New York University, New York, NY 10016, USA

[5]Present address: Neuroscience and Mental Health Institute, Department of Physiology, University of Alberta, T6G 2E2, Canada

[6]Lead contact

*Correspondence: laure.verret@univ-tlse3.fr

https://doi.org/10.1016/j.isci.2022.103895

terminals and social memory (Domínguez et al., 2019). Hence, we hypothesize that PV cell disturbances in area CA2, and more specifically, the loss of associated PNN could contribute to social memory deficits in the Tg2576 mouse model of AD.

Neuregulin-1 (NRG1) is a growth factor involved in experience-dependent maturation of PV neurons through the activation of the ErbB4 receptor in the postnatal brain (Mei and Nave, 2014; Sun et al., 2016). For instance, maturation of PV neurons during the critical period of ocular dominance depends on the activation of the NRG1/ErbB4 pathway in the visual cortex (Gu et al., 2016). We have previously shown that activating NRG1/ErbB4 signaling is critical for the emergence of iLTD and social memory (Domínguez et al., 2019). Therefore, we now postulate that local administration of exogenous NRG1 could improve PV cell function and/or enhance PNN formation in area CA2 in the context of AD.

Here we confirm that although Tg2576 mice exhibit normal sociability, their social recognition and social memory capacities are deeply impaired. Noticeably, these behavioral deficits are concomitant with decreased expression of both PV and PNN in area CA2, as well as a reduction of associated long-term plasticity. Furthermore, local injection of NRG1 rescues the number of PV and PV/PNN cells detectable in the area CA2 of Tg2576 mice. Strikingly, AD mice injected with NRG1 in area CA2 display normal performance on social memory tests. Therefore, we demonstrate that disruption of PNN around PV interneurons in area CA2 might play a causal role in the social memory deficit of the Tg2576 mouse model of AD, and that their local activation with NRG1 is sufficient to restore normal social memory capacity.

RESULTS

Reduced number of PV + cells associated to PNN loss in the area CA2 of Tg2576 mice

To further characterize PV cell depletion in area CA2 associated with AD pathology, we used stereology to estimate the absolute number of PV+ cells in the different layers in area CA2 of naive 9-month-old Tg2576 and NTg mice (Figures 1A, S1A, and S1B). In agreement with our previous study (Cattaud et al., 2018), the estimated absolute number of PV+ cells was decreased in area CA2 of Tg2576 mice compared to NTg (NTg: 558.6 $\pm$ 31.12 cells; Tg2576: 387.1 $\pm$ 52.90 cells; two-sided unpaired t test: $p = 0.0163$; Figure 1A). Furthermore, the number of PV cells harboring PNN (PV+/PNN+) was dramatically reduced in area CA2 of Tg2576 mice compared to age-matched NTg mice (NTg: 478.6 $\pm$ 25.02 cells; Tg2576: 282.9 $\pm$ 40.16 cells; two-sided unpaired t test: $p = 0.0014$; Figures 1B, S1A and S1C), as well as the overall intensity of WFA fluorescence (Figure S1D). Noticeably, this was associated with lower intensity of PV staining in PV+ cells of Tg2576 mice (Mann-Whitney test, $p = 0.001$; Figures 1C and 1D), suggesting that the diminished PNN presence in area CA2 of AD mice is accompanied by a reduced activity of PV interneurons (Donato et al., 2013; Favuzzi et al., 2017; Yamada et al., 2015).

Inhibitory transmission and PV-dependent long-term plasticity are altered in area CA2 of Tg2576 mice

In the healthy adult brain, inhibitory transmission in area CA2 exerts a powerful control on the excitatory inputs from the Schaffer collaterals (SC), preventing CA3 inputs to evoke action potential firing in CA2 pyramidal neurons (Chevaleyre and Siegelbaum, 2010). To determine whether the observed decrease in PV density in Tg2576 mice affects inhibitory transmission and its control of excitatory inputs, we first recorded postsynaptic potentials (PSP) in CA2 pyramidal neurons after stimulating CA3 inputs. In NTg mice, the amplitude of the depolarizing phase of the PSPs was small because of the large feedforward inhibition. In Tg2576, the depolarizing phase of the PSP was much larger and the following hyperpolarization was nearly absent (two-way ANOVA with repeated measures for trial: $p = 0.037$; Figure 2A). This change in PSP amplitude could result from an increased excitatory drive or from a decrease in inhibitory transmission. To address this, we first used extracellular recording to monitor the strength of excitatory transmission. We measured the slope of the rising phase of the field potential in response to CA3 input stimulation (a parameter not affected by inhibitory transmission) and normalized it to the fibber volley (a measure of the number of axons recruited by the stimulation). We found no difference between NTg and Tg2576 mice (NTg: 0.775 $\pm$ 0.108, Tg2576: 0.780 $\pm$ 0.115, 2-sample t test: $p = 0.972$; Figure S2A). This result indicates that excitatory transmission is not significantly altered in Tg2576 mice and that the change in PSP amplitude recorded in the whole cell likely results from a decrease in inhibitory transmission. Therefore, we performed two experiments to determine whether inhibitory transmission was indeed reduced in Tg2576 mice. First, we isolated inhibitory postsynaptic current (IPSC) in presence of ionotropic glutamatergic receptor blockers and recorded the paired-pulse ratio (PPR, a measure of the release probability of GABA) of two

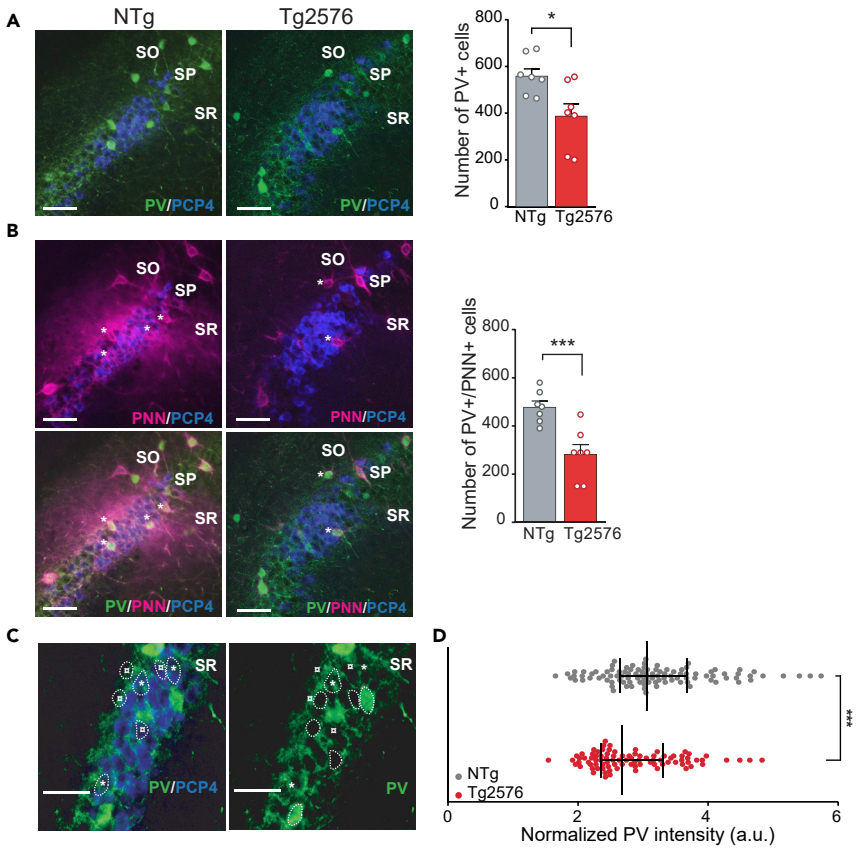

Figure 1. Reduced number of PV+ cells associated with PNN loss in the area CA2 of Tg2576 mice

(A) Stainings for PV (green) and PCP4 (blue) in area CA2 of 9-month-old NTg and Tg2576 mice (left) and stereological estimation of PV+ cells in area CA2 (right) reveal reduced numbers of PV+ cells in Tg2576 (n = 7) compared to NTg (n = 7) mice. *: $p < 0.05$, unpaired t test between genotypes.

(B) Stainings for WFA (PNN, magenta) and PCP4 (blue) in area CA2 and stereological estimation of absolute number indicate a decrease of PV+/PNN+ cells in area CA2 of Tg2576 (n = 7) compared to NTg (n = 7) mice. ***: $p < 0.005$, unpaired t test between genotypes.

(C) For assessment of PV intensity in area CA2, PV intensity of fluorescence of PV-/PCP4+ pyramidal neuron soma (dotted lines with ¤) is used as baseline for normalization of PV intensity of PV+/PCP4- cells (with *).

(D) Normalized PV intensity in the soma of PV+ cells from SP of area CA2 shows lower PV signal in PV+ cells of Tg2576 mice (n = 89 cells from seven mice) compared to those of NTg mice (n = 102 cells from seven mice). Bars represent the median with interquartiles and each dot represents a PV+ cell. ***: $p < 0.005$ between genotype, Mann-Whitney test. (A and B) Bar graphs represent the mean and error bars the SEM Scale bars = 50 μm. See also Figure S1.

consecutive IPSCs. We found that the PPR was much larger in Tg2576 compared to NTg mice (Tg2576: 0.777 ± 0.031; NTg: 0.522 ± 0.027; 2-sample t test, $p < 0.0001$; Figure 2B), indicating that GABA release probability was reduced in Tg2576 mice. Next, we recorded the frequency and amplitude of spontaneous IPSCs. We found that the frequency of spontaneous IPSCs was strongly reduced in Tg2576 mice (NTg: 21.5 ± 2.3 Hz; Tg2576: 13.5 ± 1.7Hz; 2-sample t test: $p = 0.017$, Figure S2B), but the amplitude was similar between genotypes (NTg: 32.9 ± 2.7 pA; Tg2576: 29.3 ± 3.7 pA; 2-sample t test: 0.345, Figure S2B). This result confirms that GABA release probability was reduced in Tg2576 mice. We then asked whether this decrease in inhibitory transmission was sufficient to reveal action potential firing in CA2 pyramidal neurons when stimulating CA3 inputs. Using field potential recordings, we found that stimulation of CA3 inputs resulted in population spikes in Tg2576 but not in NTg mice (two-way ANOVA with repeated measures for genotype: $p = 0.030$; Figure 2C). As we did not detect any change in either resting membrane potential or action potential threshold of CA2 pyramidal neurons (resting potential: NTg: −73.5 ± 1.0mV; Tg2576: −73.6 ± 1.0mV; 2-sample t test: $p = 0.958$; action potential threshold: NTg: −47.9 ± 2.2mV; Tg2576: −46.8 ± 1.6mV; 2-sample t test: $p = 0.671$; Figures S2C and S2D), we concluded that this increased action potential firing likely resulted from a change in inhibitory transmission.

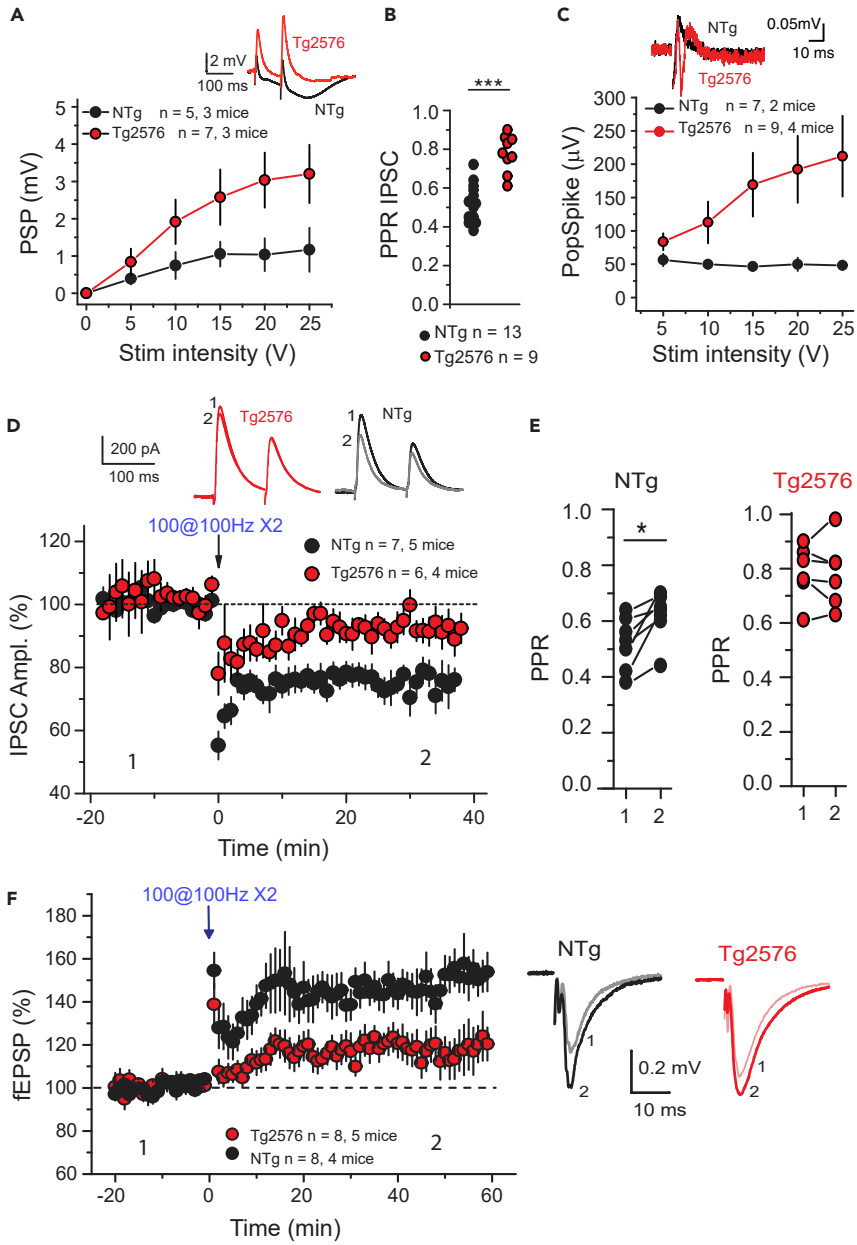

Figure 2. Inhibitory transmission and PV-dependent long-term plasticity are altered in area CA2 of Tg2576 mice

(A) Whole-cell recordings of CA2 pyramidal neurons during stimulation of CA3 axons reveal an increased amplitude of the postsynaptic potential (PSP), a composite of excitatory and inhibitory potentials, in slices prepared from Tg2576 mice (red) as compared to those of NTg mice (black). Average sample traces are shown on top.

(B) The paired-pulse ratio (PPR) of two inhibitory postsynaptic currents (IPSC) recorded in CA2 neurons with CA3 axonal stimulation is increased in slices of Tg2576 as compared to NTg mice.

(C) Averaged population spike (PS) amplitudes measured extracellularly in the pyramidal layer of area CA2 reveal that stimulation of CA3 inputs more readily results in action potential firing in Tg2576 than in NTg mice. Average sample traces are shown on top.

(D) The time course of normalized IPSC amplitudes recorded in CA2 pyramidal neurons before and after high frequency stimulations indicates that iLTD can be triggered in slices of NTg mice but only a transient depression is observed in Tg2576 mice.

(E) Averaged sample traces at the time indicated by number are shown on top. (E) The PPR of two IPSCs recorded in CA2 pyramidal neurons is increased following HFS (2) in samples prepared from NTg mice (black, left) (n = 6 recordings from four mice), but remains unchanged between before (1) and after (2) HFS in Tg2576 mice (red, right).

Figure 2. *Continued*
(F) Amplitude of the field excitatory PSP in area CA2 shows a smaller increase following a high-frequency stimulation in Tg2576 compared to NTg mice.
Average sample traces of fEPSP at the time indicated by number are shown on the right. See also Figure S2.

We next asked whether PV-dependent long-term plasticity was affected in Tg2576 mice (Domínguez et al., 2019; Piskorowski and Chevaleyre, 2013). Whole-cell patch clamp recordings of area CA2 pyramidal cells were performed in order to measure IPSCs evoked by SC stimulation. Following a high-frequency stimulation (HFS), we observed iLTD in area CA2 of NTg animals (74.1 ± 4.1% of baseline; Figure 2D). In contrast, the same stimulation only induced a small depression of IPSC amplitude in Tg2576 mice (90.9 ± 3.8% of baseline; Figure 2D) that was significantly lower than that evoked in NTg mice (2-sample t test: $p = 0.013$). In agreement with the presynaptic locus of iLTD, the HFS was followed by a significant increased PPR in area CA2 of NTg mice (from 0.52 ± 0.03 to 0.62 ± 0.03, paired t test: $p = 0.010$; Figure 2E, left), but not in hippocampal slices from Tg2576 mice (from 0.78 ± 0.04 to 0.78 ± 0.05, paired t test: $p = 0.822$; Figure 2E, right). Finally, iLTD in area CA2 has been found to result in a large increase in the overall net PSP amplitude through a disinhibitory mechanism (Nasrallah et al., 2015). In agreement with the reduced iLTD, we observed that a HFS resulted in a much smaller increase in PSP amplitude in Tg2576 (115.9 ± 8.9%) compared to NTg mice (153.6 ± 7.4%, 2-sample t test: $p = 0.006$; Figure 2F).

Social recognition and social memory are impaired in Tg2576 mice

The fact that inhibitory transmission and resulting plasticity are altered in area CA2 of Tg2576 mice strongly suggests that social recognition and social memory might be altered in this mouse model of AD (Domínguez et al., 2019; Leroy et al., 2017). To assess social recognition and social memory capacities of 9-month-old Tg2576 mice, we first determined that they demonstrate normal sociability (two-way ANOVA with repeated measures for chambers: $p < 0.0001$; for genotype: $p = 0.9834$; interaction: $p = 0.5966$; Sidak's post-hoc test for empty chamber vs familiar mouse: NTg: 56.58 ± 9.84 s vs 14.20 ± 3.76 s, $p = 0.0002$; Tg2576: 59.78 ± 8.36 s vs 10.69 ± 2.30 s, $p < 0.0001$; Figure 3A). However, when confronted with a choice between a familiar and a novel mouse, Tg2576 mice did not show significant preference for the unfamiliar individual (two-way ANOVA with repeated measures for chambers: $p < 0.0001$; for genotype: $p = 0.3151$; interaction: $p = 0.0038$; Sidak's post hoc test for familiar vs new mouse: 30.51 ± 4.45 s vs 41.27 ± 5.44 s, $p = 0.1180$; Figure 3B), revealing that their social recognition is impaired.

We then examined the ability of Tg2576 mice to form social memory with the 5-trial test (Domínguez et al., 2019; Kogan et al., 2000) (Figure 3C). As expected, NTg and Tg2576 behaved differently during four subsequent exposures to the same mouse (two-way ANOVA with repeated measures for trial: $p < 0.0001$; for genotype: $p = 0.0140$; interaction: $p < 0.0001$; Figure 3C). When a novel mouse was introduced (trial 5), NTg mice showed an expected rebound of interaction time, whereas Tg2576 mice still displayed the same amount of interaction (Figures 3C and 3D). As olfactory functions—crucial for social discrimination in mice—have been described to be impaired early in this mouse model of AD (Guerin et al., 2009), we performed a test to ensure that Tg2576 mice retained the ability to habituate and discriminate different odors (Yang and Crawley, 2009). Importantly, both NTg and Tg2576 mice were able to discriminate and habituate to both social and nonsocial odors (Figure S3), indicating that the inability to form social memory cannot be attributed to olfactory deficits in AD mice. These results indicate that social recognition and social memory, but not sociability, are impaired in 9-month-old Tg2576 mice.

PNN disruption in area CA2 is sufficient to decrease PV presence and to abolish social memory capacity

We previously demonstrated that the presence of PNN around PV cells in area CA2 is critical to the emergence of both iLTD and social memory capability (Domínguez et al., 2019). Hence, we hypothesized that PV and PNN loss in this hippocampal area is contributing to social memory deficits in the Tg2576 mouse model of AD. To test this hypothesis, we performed bilateral injections of a vehicle (PBS) or Chondroitinase-ABC (ChABC) solution into area CA2 of female wild-type C57BL/6J (WT) mice. Seven days later, the intensity of the PNN staining was significantly decreased in area CA2 following ChABC injection (PBS: 29.46 ± 3.21 a.u.; ChABC: 17.19 ± 2.07 a.u.; $p = 0.0022$, two-sided unpaired t test, Figures 4A and S4). Interestingly, although the estimated absolute number of PV+ cells in area CA2 pyramidal layer was not modified by ChABC injection (Figure S4), this was associated with lower intensity of PV staining in PV+ cells of ChABC

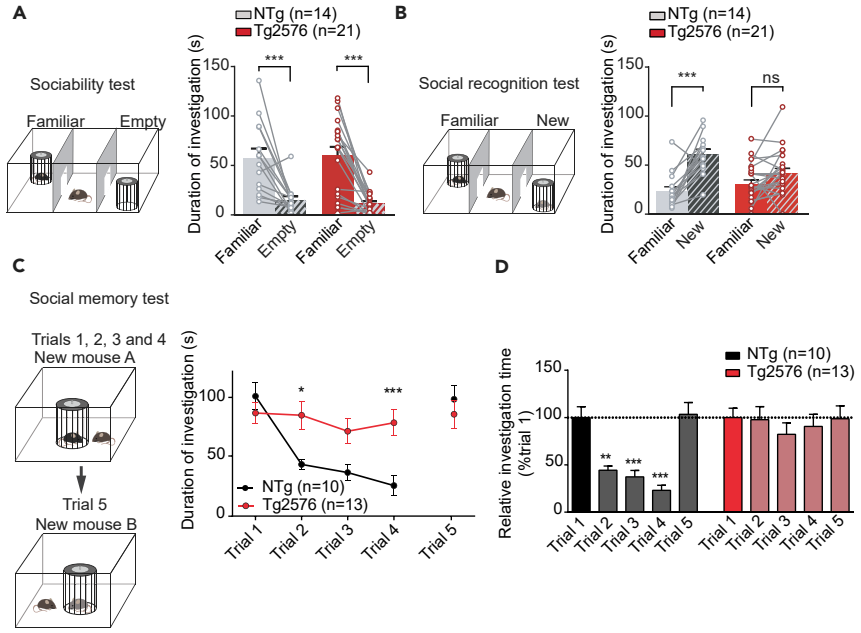

Figure 3. Social recognition and social memory are impaired in Tg2576 mice

(A) Sociability test in the 3-chamber paradigm indicates that mice from both genotypes spend more time with a conspecific than an empty cage. ***: $p < 0.005$ repeated-measures two-way ANOVA followed by Sidak's post hoc test between cages.

(B) Social recognition test reveals that NTg mice spend more time with a new mouse than with the familiar one, whereas Tg2576 mice spend an equal amount of time with both mice. ***: $p < 0.005$ repeated-measures two-way ANOVA followed by Sidak's post hoc test between cages.

(C) Social memory assessed with the 5-trial test reveals impairment in Tg2576 mice. *: $p < 0.05$, ***: $p < 0.005$ between trials for NTg and Tg2576 mice, repeated-measures two-way ANOVA followed by Sidak's post hoc test.

(D) Normalized measures show that the investigation time of NTg mice decreases significantly from trial two to 4. In contrast, no significant change in investigation time is observed across trials in Tg2576 mice. Repeated-measures one-way ANOVA followed by Sidak's post hoc test. **$p < 0.01$ and ***$p < 0.005$ between trial n and trial 1. Bar graphs represent the mean and error bars SEM See also Figure S3.

mice (Mann-Whitney test, $p < 0.0001$; Figure 4B), suggesting again that the loss of PNN in area CA2 induces a decrease in PV cell activity.

Local injection of ChABC in area CA2 of female WT mice resulted in impaired social memory (two-way ANOVA with repeated measures for trial: $p < 0.0001$; for treatment: $p = 0.0024$; interaction: $p = 0.0105$; n = 10 PBS-injected and 12 ChABC-injected mice; Figures 4C and 4D). Here, we confirmed that degradation of the PNN in area CA2 is sufficient to preclude the formation of social memory, consistent with our findings using male mice (Domínguez et al., 2019).

Local NRG1 restores PV+/PNN+ cells and social memory formation in Tg2576 mice

In order to demonstrate that disruption of PNN and PV interneuron function in area CA2 plays a pivotal role in social memory deficits of the Tg2576 mouse model of AD, we aimed at increasing PV cell activity and/or PNN presence locally in area CA2 of Tg2576 mice. To do so, we used bilateral CA2 injections of a control (PBS) or NRG1 solution in NTg and Tg2576 mice (Figure 5A). Noticeably, 5 days following local injections, we observed an increased number of detectable PV+ cells in area CA2 of Tg2576 mice injected with NRG1 (556.0 $\pm$ 27.94 cells) compared to PBS-injected Tg2576 mice (390.9 $\pm$ 43.73 cells; two-way ANOVA for injection: $p = 0.0042$; for genotype: $p = 0.0006$; interaction: $p = 0.3511$; Sidak's post hoc test Tg2576-PBS vs Tg2576-NRG1: $p = 0.0412$; Figure 5A), totally abolishing the differences between genotypes (NTg-PBS mice, 586.0 $\pm$ 47.89 cells; Sidak's post hoc test NTg-PBS vs Tg2576-NRG1: $p = 0.9967$; Figure 5A). This rescue was mainly because of an effect in the SP (Figure S5A). The increased number of PV+ cells following NRG1 injection was accompanied by a restored presence of PNN around PV cells in Tg2576 (344.0 $\pm$ 29.78 cells) compared to NTg mice (425.0 $\pm$ 44.78 cells; two-way ANOVA for injection: $p = 0.0101$; for genotype:

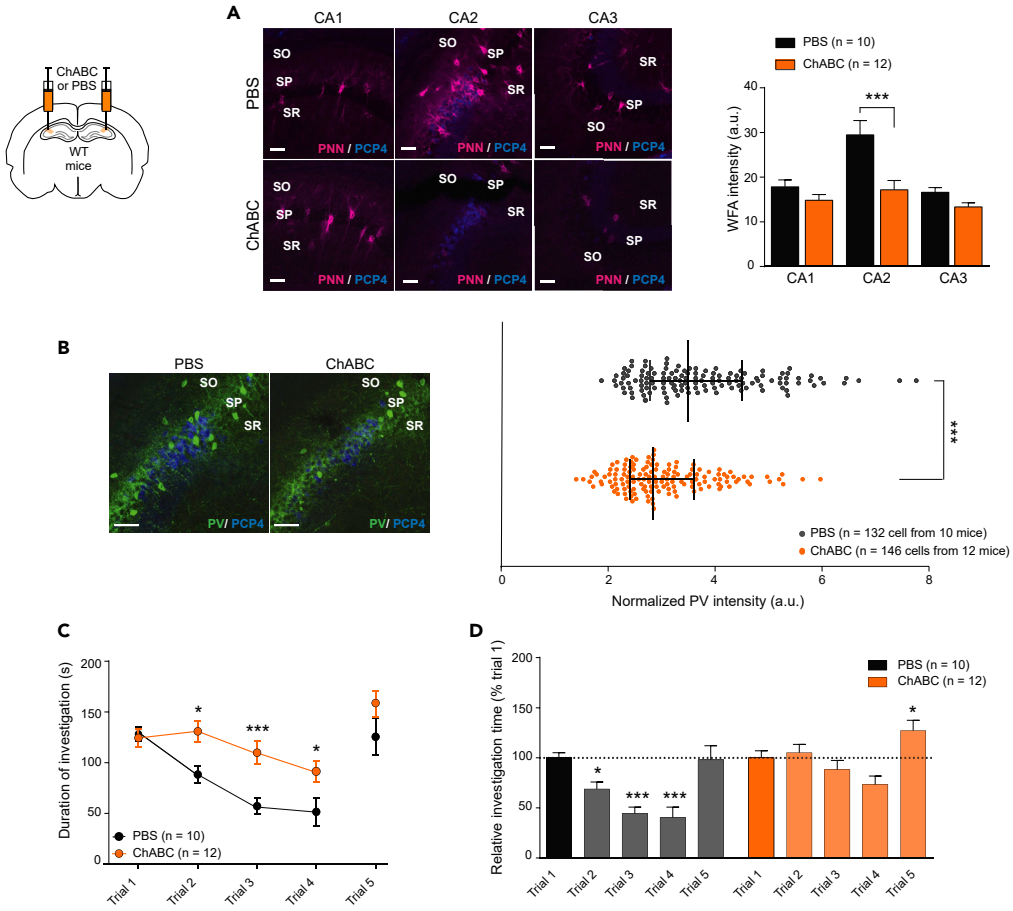

Figure 4. PNN disruption in area CA2 is sufficient to decrease PV presence and to abolish social memory capacity

(A) Staining for WFA (PNN, magenta) 7 days after local injections of PBS or ChABC solution in area CA2 shows a large decrease of PNN presence in area CA2 (***: $p < 0.005$ for unpaired t test with Bonferroni's correction for multiple comparisons between treatment), while sparing CA1 and CA3 areas.

(B) Parvalbumin intensity in PV+ cells from SP of area CA2 is reduced after ChABC injection. Bars represent the median with interquartiles and each dot represents a PV+ cell. ***: $p < 0.0001$, Mann-Whitney test.

(C) The total duration of investigation of an unknown mouse reveals alteration of social memory formation in WT mice following ChABC injection in area CA2. *: $p < 0.05$, ***: $p < 0.005$ between trials for NTg and Tg2576 mice, RM two-way ANOVA followed by Sidak's post hoc test.

(D) Normalized data show a significant decrease of the investigation time of PBS mice from trial two to 4. In contrast, no significant change in investigation time is observed in ChABC mice. *$p < 0.05$, ***$p < 0.005$ between trial n and trial 1, repeated-measures one-way ANOVA followed by Sidak's post hoc test. (A, C, and D) Bar graphs represent the mean and error bars the SEM. Scale bar = 50 μm. See also Figure S4.

$p < 0.0001$; interaction: $p = 0.3642$; Sidak's post hoc test NTg-PBS vs Tg2576-NRG1: $p = 0.4455$; Figure 5B). Nonetheless, it did not induce an increase of PNN presence around non-PV neurons (NTg-PBS: 30.00 ± 9.19 cells; NTg-NRG1: 45.00 ± 6.87 cells; Tg2576-PBS: 17.27 ± 3.84 cells; Tg2576-NRG1: 24.00 ± 6.18 cells; Figures S5C–S5F). Noticeably, we observed a significantly higher intensity of PV staining in PV+ cells following NRG1 injection in area CA2 of Tg2576 mice, again abolishing the differences between genotypes (Kruskal-Wallis and Dunn's post hoc test Tg2576-PBS vs Tg2576-NRG1: $p < 0.0001$; NTg-PBS vs Tg2576-NRG1: $p = 0.7363$; Figure 5C). This change in PV expression following NRG1 injection suggests that NRG1 has promoted the maturation of PNN around PV+ cells specifically and/or triggered an increase of activity of PV interneurons in area CA2 of Tg2576 mice.

Five days after intra-CA2 injections of NRG1 or PBS solution, mice from the four experimental groups were subjected to the 5-trial social memory test. We observed that Tg2576-PBS mice showed the same deficit in

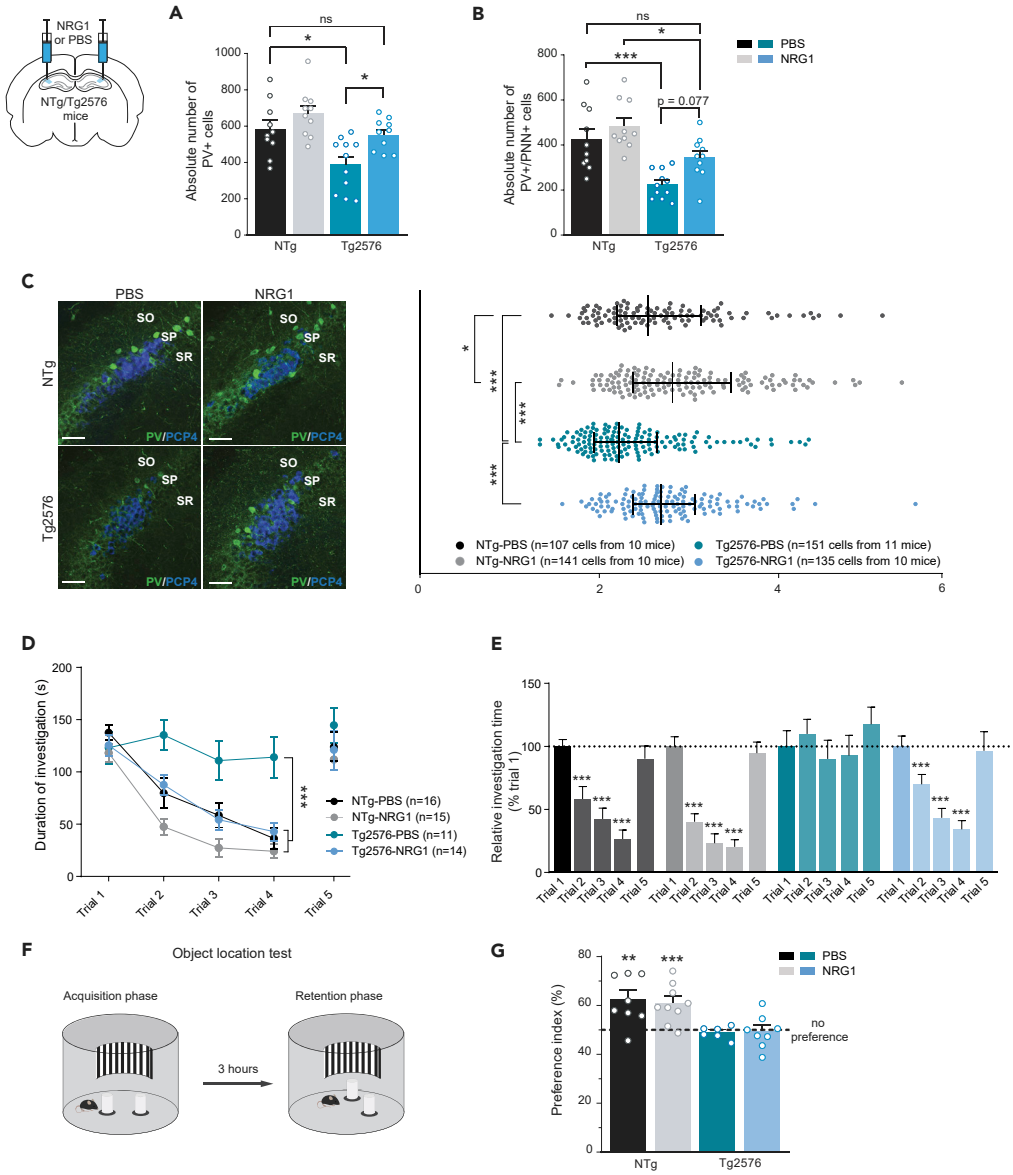

Figure 5. Local NRG1 restores PV+/PNN+ cells and social memory formation in Tg2576 mice

(A) Quantification of PV+ cells 5 days after NRG1 injection in area CA2 reveals a restoration of the number of detectable PV+ cells in area CA2 of Tg2576 mice injected with NRG1 compared to Tg2576-PBS mice, abolishing the difference between genotypes. *: $p < 0.05$, ***: $p < 0.005$, two-way ANOVA followed by Sidak's post hoc test.

(B) The increased number of PV+ cells following NRG1 injection was accompanied by a restored presence of PNN around PV cells in Tg2576 mice compared to NTg ones. **: $p < 0.05$, ***: $p < 0.005$, ns: $p > 0.05$, two-way ANOVA followed by Sidak's post hoc test.

(C) PV intensity of the soma of PV+ cells from area CA2 SP shows that PV signal is higher in PV+ cells of Tg2576-NRG1 mice compared to those of Tg2576-PBS mice. Bar represents the median and interquartiles and each dot represents one PV+ cell. *: $p < 0.05$, ***: $p < 0.005$, Kruskal-Wallis followed by Dunn's post hoc test.

(D) Social memory test indicates that local injections of NRG1 in area CA2 induce a restoration of social memory formation in Tg2576 mice. ***: $p < 0.005$ repeated-measures two-way ANOVA.

(E) Normalized data relative to mean interaction time during trial one shows a significant decrease in investigation time in Tg2576 mice injected with NRG1 from trial two to four similar of NTg groups. In contrast, no significant change in investigation time is observed in Tg2576 mice injected with PBS. ***$p < 0.005$ between trial n and trial 1, repeated-measures one-way ANOVA followed by Sidak's post hoc test.

(F) Spatial memory was assessed with an object location test.

Figure 5. *Continued*
(G) Preference index of the investigation time between displaced and fixed object during retention phase indicate that spatial memory is altered in Tg2576 mice, even following NRG1 injections. **: $p < 0.01$, ***: $p < 0.005$ for one-sample t test against chance (50%). (A, B, E, and G) Bar graphs represent the mean and error bars of the SEM See also Figure S5.

social memory as previously described (one-way ANOVA with repeated measures, Sidak's post hoc test trial n vs trial 1: $p > 0.05$ for all trials; Figure 5D). However, NRG1 injections into area CA2 accelerated social learning in mice from both genotypes compared to PBS-injected individuals (two-way ANOVA with repeated measures for trial: $p < 0.0001$; for injection: $p < 0.0001$; interaction: $p < 0.0001$; Figure 5D). Strikingly, Tg2576 mice injected with NRG1 exhibited the same learning curve as the NTg-PBS group (Figures 5D and 5E), indicating that local activation of NRG1-dependent signaling was sufficient to restore normal social memory capacity in this mouse model of AD.

Because specific manipulations of area CA2 are known to impact social memory without affecting performance in other types of hippocampal-dependent memory (Hitti and Siegelbaum, 2014), we used another cohort of mice to address whether NRG1 injection in area CA2 impacted spatial memory . Mice from each experimental group were subjected to the novel object location test 5 days after NRG1 or saline injection into area CA2 (Figure 5F). During the test, NTg mice showed a preference for the displaced object, independent of their treatment (one-sample t test vs chance: NTg-PBS: $p = 0.0097$; NTg-NRG1: $p = 0.0033$; Figure 5G). In contrast, all Tg2576 mice spent a similar amount of time exploring the displaced and the fixed objects, regardless of treatment with NRG1 (one-sample t test vs chance: Tg2576-PBS: $p = 0.5097$; Tg2576-NRG1: $p = 0.8457$; Figure 5G), indicating that spatial memory remained impaired in Tg2576 mice. Therefore, activation of NRG1-dependent signaling in area CA2 is able to restore social memory, but not spatial memory, of Tg2576 mice.

DISCUSSION

Our study shows that disruption of PNN around PV interneurons in area CA2 of the Tg2576 mouse model of AD plays a pivotal role in reduced inhibitory control and plasticity in this hippocampal area, and that these deficits are linked to social memory impairments. Furthermore, local injection of NRG1 is sufficient to enhance PV and PNN presence in area CA2 of Tg2576 mice, as well as restore social memory capacity in this AD mouse model.

Our study indicates that 9-month-old Tg2576 mice have a reduced number of PV+ interneurons and PV+/PNN+ cells in area CA2. This agrees with previous work showing the same deficits in area CA2 of Tg2576 mice at 6 months of age (Cattaud et al., 2018). Moreover, the reduced number of PV+ cells and PNN in area CA2 of Tg2576 mice is associated with decreased intensity of PV staining in PV+ cells. As PV content is positively correlated with both PV cell activity and GABA release (Donato et al., 2013; Favuzzi et al., 2017; Yamada et al., 2015), this finding is in accordance with the idea that PV cell activity is reduced in the Tg2576 mouse model of AD, and that PNN absence around PV cells contributes to this reduced neuronal activity. As such, our findings suggest that the lack of PNN around PV cells leads to low neuronal activity associated with low PV protein content, rather than triggering the loss of these interneurons, because of disrupted protection against oxidative stress, for instance (Cabungcal et al., 2013; Suttkus et al., 2012). The approximate increase of about 40% of detectable PV+ neurons 5 days after NRG1 injection supports this idea.

Notably, we described that these PV/PNN modifications are associated with reduced inhibitory control in area CA2 of Tg2576 mice, resulting in hyperexcitability of pyramidal neurons within this hippocampal area. As a consequence, iLTD is also strongly impaired, demonstrating for the first time that this PV-dependent long-term plasticity is dysfunctional in a mouse model of AD. A loss of PV interneuron density was also reported in area CA2 of a mouse model of the 22q11.2 deletion syndrome, which is linked with elevated schizophrenia diagnosis (Piskorowski et al., 2016). In contrast to the Tg2576 mouse model, this was also accompanied by a significant reduction in the resting membrane potential of CA2 pyramidal neurons, reducing the output of area CA2 and likely impacting social memory. Hence, although the loss of PV cells in these two pathological conditions has opposite effect on CA2 output activity, both mouse lines show impaired social memory. This highlights the fact that physiological activity of area CA2 is required to form social memory—directly and/or through its projections to ventral CA1 (Meira et al., 2018) —, and that local PV cells, by maintaining E/I balance, play a crucial role in the maintenance of such physiological activity.

Hence, 9-month-old Tg2576 mice devoid of plaques show deep anatomical and functional changes in area CA2 that may interfere with their social memory capacity. Although social memory deficits are commonly observed in AD patients, the assessment of this specific kind of memory has been poorly explored in AD mouse models. To our knowledge, only one study addressed this question, revealing impaired social memory in very old female Tg2576 mice (22–23 months old) (Deacon et al., 2009). Our findings indicate that the Tg2576 mouse model does not have impaired sociability, but that social recognition and social memory are both affected.

Interestingly, the anatomical and functional properties of area CA2 of 9-month-old Tg2576 mice are reminiscent of those observed in juvenile mice. Indeed, young mice also present low PNN in area CA2 associated with the inability to induce iLTD and to form social memory until late adolescence (Domínguez et al., 2019). This study indicates that PNN maturation during late adolescence controls the emergence of PV-dependent long-term plasticity in area CA2, and that activation of the tyrosine kinase receptor ErbB4 with endogenous NRG1 is required for iLTD induction. Our findings show that a single local injection of NRG1 is sufficient to restore social memory capacity in the Tg2576 mouse model of AD, and that this is associated with a recovery of the PV/PNN network in area CA2.

The growth factor NRG1 is essential for the development of the nervous system. NRG1 drives the experience-dependent maturation of cortical and hippocampal networks through the activation of its receptor ErbB4, which is densely expressed by PV interneurons (Fazzari et al., 2010; Mei and Nave, 2014; Mei and Xiong, 2008). During normal postnatal development, activity-dependent NRG1/ErbB4 signaling regulates excitatory inputs onto PV cells, probably through the stabilization of synaptic glutamatergic AMPA receptors, and thus permits synaptic plasticity and maturation to occur (Li et al., 2007; Sun et al., 2016). Interestingly, NRG1/ErbB4 activation attenuates the Aβ-induced LTP impairment in hippocampal slices (Min et al., 2011). NRG1 infusion for one month into the lateral ventricle of 12-month-old Tg2576 mice was shown to improve their spatial learning and memory, associated with increased dendritic spine density in area CA1 (Ryu et al., 2016). NRG1 activity is highly dependent on its cleavage by the β-secretase BACE1, which is also responsible for the production of Aβ-peptide through the cleavage of APP (Mei and Xiong, 2008). It is thus possible that the beneficial effect of NRG1 in the context of AD is because of shifting BACE1 activity toward NRG1 instead of APP cleavage, leading to reduced amyloidopathy. However, here we show that a single NRG1 local injection is sufficient for inducing changes of PV/PNN network lasting at least 5 days, and able to sustain recovery of a specific cognitive function. This suggests that the beneficial effects of NRG1 are more likely because of long-lasting changes of PV cell function and associated synaptic plasticity rather than reduced local amyloid charge. Many studies suggest the existence of a positive feedback relationship between synaptic activity induced by experience and NRG1 signaling (Li et al., 2007; Sun et al., 2016). It is indeed possible that, in the context of AD, reduced PV cell activity is associated with downregulation of NRG1 signaling. Thus, a single boost of NRG1 may be sufficient to trigger PV cell function in a way that experience-dependent activity will be rescued. We have previously shown that a transient exposure to an environment with high social and sensory stimulations is sufficient to restore PV/PNN presence in the hippocampus of Tg2576 mice (Cattaud et al., 2018), and to induce long-lasting beneficial effect on their memory performance (Verret et al., 2013). It is thus possible that exposure to an enriched environment has provided the trigger necessary to enhance synaptic maturation of PV cells through NRG1-experience-dependent activity. This also suggests that the beneficial effects of NRG1 on the PV/PNN network of Tg2576 mice might not be specific to area CA2 and social memory, and could be generalized to other brain areas in which other cognitive functions rely.

Altogether, our work underpins the critical role of PNN-enwrapped PV cells of area CA2 in social memory deficits of the Tg2576 mouse model of AD. Importantly, local stimulation of NRG1 signaling is sufficient to restore PNN presence around PV cells, and normal social memory. This indicates that promoting experience-dependent PV cell activity, whether it is with environmental simulations (Cattaud et al., 2018; Iaccarino et al., 2016; Martorell et al., 2019), or by mimicking their impact by activating pro-maturation pathways such as NRG1/ErbB4, can be used to tackle AD-related cognitive deficits.

Limitations of the study

Our study was conducted using female mice only. Social memory tests involve interaction of mice arising from different cages and litters. Tg2576 males have been reported to be significantly more aggressive than their non-transgenic littermates; with aging, their cohabitation becomes difficult because it triggers fighting,

aggressive behavior, and stress. Hence, they usually need to be isolated from their littermate, which is prohibitive for social memory tests.

STAR★METHODS

Detailed methods are provided in the online version of this paper and include the following:

- KEY RESOURCES TABLE
- RESOURCE AVAILABILITY
  - Lead contact
  - Materials availability
  - Data and code availability
- EXPERIMENTAL MODEL AND SUBJECT DETAILS
- METHOD DETAILS
  - Stereotaxic injections
  - Behavioral experiments
  - Tissue preparation and immunohistochemistry
  - Image analysis
  - Electrophysiological recordings
- QUANTIFICATION AND STATISTICAL ANALYSIS

SUPPLEMENTAL INFORMATION

Supplemental information can be found online at https://doi.org/10.1016/j.isci.2022.103895.

ACKNOWLEDGMENTS

The authors thank Lionel Moulédous and Daniel H. Kim for critically reading the article, and Stéphane Pech for animal care and technical help. Mice were housed in the ABC Facility of ANEXPLO, Toulouse. The authors greatly acknowledge the Mouse Behavioral Core (MBC) of the Center of Integrative Biology. This work was supported by the Centre National de la Recherche Scientifique, the University of Toulouse, and by the Association France Alzheimer and the Institut Universitaire de France. Graphical abstract was created with BioRender.com.

AUTHOR CONTRIBUTIONS

Conceptualization, C.C.R., V.Ch., and L.V.; Investigation, C.C.R., V.R., G.B., M.L., S.L., V.Ch., and V.Ca.; Writing – Original Draft, V.Ch. and L.V.; Writing – Review & Editing, C.C.R., V.R., G.B., R.A.P., C.R., V.Ch., and L.V.; Funding Acquisition, C.R. and L.V.; Resources, C.L.; Supervision, V.Ch. and L.V.

DECLARATION OF INTERESTS

The authors declare no conflict of interests.

Received: August 9, 2021
Revised: December 7, 2021
Accepted: February 7, 2022
Published: March 18, 2022

REFERENCES

Botcher, N.A., Falck, J.E., Thomson, A.M., and Mercer, A. (2014). Distribution of interneurons in the CA2 region of the rat hippocampus. Front. Neuroanat. *8*, 104. https://doi.org/10.3389/fnana.2014.00104.

Cabungcal, J.H., Steullet, P., Morishita, H., Kraftsik, R., Cuenod, M., Hensch, T.K., and Do, K.Q. (2013). Perineuronal nets protect fast-spiking interneurons against oxidative stress. Proc. Natl. Acad. Sci. U S A *110*, 9130–9135. https://doi.org/10.1073/pnas.1300454110.

Canning, D.R., McKeon, R.J., DeWitt, D.A., Perry, G., Wujek, J.R., Frederickson, R.C., and Silver, J. (1993). beta-Amyloid of Alzheimer's disease induces reactive gliosis that inhibits axonal outgrowth. Exp. Neurol. *124*, 289–298. https://doi.org/10.1006/exnr.1993.1199.

Carstens, K.E., Phillips, M.L., Pozzo-Miller, L., Weinberg, R.J., and Dudek, S.M. (2016). Perineuronal nets suppress plasticity of excitatory synapses on CA2 pyramidal neurons. J. Neurosci. *36*, 6312–6320. https://doi.org/10.1523/JNEUROSCI.0245-16.2016.

Cattaud, V., Bezzina, C., Rey, C.C., Lejards, C., Dahan, L., and Verret, L. (2018). Early disruption of parvalbumin expression and perineuronal nets in the hippocampus of the Tg2576 mouse model of Alzheimer's disease can be rescued by enriched environment. Neurobiol. Aging *72*, 147–158. https://doi.org/10.1016/j.neurobiolaging.2018.08.024.

Celio, M.R. (1993). Perineuronal nets of extracellular matrix around parvalbumin-containing neurons of the hippocampus. Hippocampus *3*, 55–60.

Chevaleyre, V., and Siegelbaum, S.A. (2010). Strong CA2 pyramidal neuron synapses define a powerful disynaptic cortico-hippocampal loop. Neuron *66*, 560–572. https://doi.org/10.1016/j.neuron.2010.04.013.

Deacon, R.M., Koros, E., Bornemann, K.D., and Rawlins, J.N. (2009). Aged Tg2576 mice are impaired on social memory and open field habituation tests. Behav. Brain Res. *197*, 466–468. https://doi.org/10.1016/j.bbr.2008.09.042.

Domínguez, S., Rey, C.C., Therreau, L., Massotte, D., Verret, L., Piskorowski, R., and Chevaleyre, V. (2019). Maturation of PNN and ErbB4 signaling in area CA2 during adolescence underlies the emergence of Parvalbumin interneuron plasticity and social memory. Cell Rep. *29*, 1099–1112.e4. https://doi.org/10.1016/j.celrep.2019.09.044.

Donato, F., Rompani, S.B., and Caroni, P. (2013). Parvalbumin-expressing basket-cell network plasticity induced by experience regulates adult learning. Nature *504*, 272–276. https://doi.org/10.1038/nature12866.

Favuzzi, E., Marques-Smith, A., Deogracias, R., Winterflood, C.M., Sanchez-Aguilera, A., Mantoan, L., Maeso, P., Fernandes, C., Ewers, H., and Rico, B. (2017). Activity-dependent gating of parvalbumin interneuron function by the perineuronal net protein brevican. Neuron *95*, 639–655.e10. https://doi.org/10.1016/j.neuron.2017.06.028.

Fazzari, P., Paternain, A.V., Valiente, M., Pla, R., Lujan, R., Lloyd, K., Lerma, J., Marin, O., and Rico, B. (2010). Control of cortical GABA circuitry development by Nrg1 and ErbB4 signalling. Nature *464*, 1376–1380. https://doi.org/10.1038/nature08928.

Gu, Y., Tran, T., Murase, S., Borrell, A., Kirkwood, A., and Quinlan, E.M. (2016). Neuregulin-dependent regulation of fast-spiking interneuron excitability controls the timing of the critical period. J. Neurosci. *36*, 10285–10295. https://doi.org/10.1523/JNEUROSCI.4242-15.2016.

Guerin, D., Sacquet, J., Mandairon, N., Jourdan, F., and Didier, A. (2009). Early locus coeruleus degeneration and olfactory dysfunctions in Tg2576 mice. Neurobiol. Aging *30*, 272–283. https://doi.org/10.1016/j.neurobiolaging.2007.05.020.

Hitti, F.L., and Siegelbaum, S.A. (2014). The hippocampal CA2 region is essential for social memory. Nature *508*, 88–92. https://doi.org/10.1038/nature13028.

Hsiao, K., Chapman, P., Nilsen, S., Eckman, C., Harigaya, Y., Younkin, S., Yang, F., and Cole, G. (1996). Correlative memory deficits, Abeta elevation, and amyloid plaques in transgenic mice. Science *274*, 99–102.

Iaccarino, H.F., Singer, A.C., Martorell, A.J., Rudenko, A., Gao, F., Gillingham, T.Z., Mathys, H., Seo, J., Kritskiy, O., Abdurrob, F., et al. (2016). Gamma frequency entrainment attenuates amyloid load and modifies microglia. Nature *540*, 230–235. https://doi.org/10.1038/nature20587.

Kogan, J.H., Frankland, P.W., and Silva, A.J. (2000). Long-term memory underlying hippocampus-dependent social recognition in mice. Hippocampus *10*, 47–56. https://doi.org/10.1002/(SICI)1098-1063(2000)10:1<47::AID-HIPO5>3.0.CO;2-6.

Leroy, F., Brann, D.H., Meira, T., and Siegelbaum, S.A. (2017). Input-timing-dependent plasticity in the hippocampal CA2 region and its potential role in social memory. Neuron *95*, 1089–1102 e5. https://doi.org/10.1016/j.neuron.2017.07.036.

Li, B., Woo, R.S., Mei, L., and Malinow, R. (2007). The neuregulin-1 receptor erbB4 controls glutamatergic synapse maturation and plasticity. Neuron *54*, 583–597. https://doi.org/10.1016/j.neuron.2007.03.028.

Martorell, A.J., Paulson, A.L., Suk, H.J., Abdurrob, F., Drummond, G.T., Guan, W., Young, J.Z., Kim, D.N., Kritskiy, O., Barker, S.J., et al. (2019). Multi-sensory gamma stimulation ameliorates Alzheimer's-associated pathology and improves cognition. Cell *177*, 256–271.e22. https://doi.org/10.1016/j.cell.2019.02.014.

Mei, L., and Nave, K.A. (2014). Neuregulin-ERBB signaling in the nervous system and neuropsychiatric diseases. Neuron *83*, 27–49. https://doi.org/10.1016/j.neuron.2014.06.007.

Mei, L., and Xiong, W.C. (2008). Neuregulin 1 in neural development, synaptic plasticity and schizophrenia. Nat. Rev. Neurosci. *9*, 437–452. https://doi.org/10.1038/nrn2392.

Meira, T., Leroy, F., Buss, E.W., Oliva, A., Park, J., and Siegelbaum, S.A. (2018). A hippocampal circuit linking dorsal CA2 to ventral CA1 critical for social memory dynamics. Nat. Commun. *9*, 4163. https://doi.org/10.1038/s41467-018-06501-w.

Min, S.S., An, J., Lee, J.H., Seol, G.H., Im, J.H., Kim, H.S., Baik, T.K., and Woo, R.S. (2011). Neuregulin-1 prevents amyloid beta-induced impairment of long-term potentiation in hippocampal slices via ErbB4. Neurosci. Lett. *505*, 6–9. https://doi.org/10.1016/j.neulet.2011.05.246.

Moy, S.S., Nadler, J.J., Perez, A., Barbaro, R.P., Johns, J.M., Magnuson, T.R., Piven, J., and Crawley, J.N. (2004). Sociability and preference for social novelty in five inbred strains: an approach to assess autistic-like behavior in mice. Genes Brain Behav. *3*, 287–302. https://doi.org/10.1111/j.1601-1848.2004.00076.x.

Nasrallah, K., Piskorowski, R.A., and Chevaleyre, V. (2015). Inhibitory plasticity permits the recruitment of CA2 pyramidal neurons by CA3(1,2,3). eNeuro *2*. https://doi.org/10.1523/ENEURO.0049-15.2015.

Nasrallah, K., Therreau, L., Robert, V., Huang, A.J.Y., McHugh, T.J., Piskorowski, R.A., and Chevaleyre, V. (2019). Routing hippocampal information flow through parvalbumin interneuron plasticity in area CA2. Cell Rep. *27*, 86–98 e3. https://doi.org/10.1016/j.celrep.2019.03.014.

Piskorowski, R.A., and Chevaleyre, V. (2013). Delta-opioid receptors mediate unique plasticity onto parvalbumin-expressing interneurons in area CA2 of the hippocampus. J. Neurosci. *33*, 14567–14578. https://doi.org/10.1523/JNEUROSCI.0649-13.2013.

Piskorowski, R.A., Nasrallah, K., Diamantopoulou, A., Mukai, J., Hassan, S.I., Siegelbaum, S.A., Gogos, J.A., and Chevaleyre, V. (2016). Age-dependent specific changes in area CA2 of the Hippocampus and social memory deficit in a mouse model of the 22q11.2 deletion syndrome. Neuron *89*, 163–176. https://doi.org/10.1016/j.neuron.2015.11.036.

Ryu, J., Hong, B.H., Kim, Y.J., Yang, E.J., Choi, M., Kim, H., Ahn, S., Baik, T.K., Woo, R.S., and Kim, H.S. (2016). Neuregulin-1 attenuates cognitive function impairments in a transgenic mouse model of Alzheimer's disease. Cell Death Dis. *7*, e2117. https://doi.org/10.1038/cddis.2016.30.

Stevenson, E.L., and Caldwell, H.K. (2014). Lesions to the CA2 region of the hippocampus impair social memory in mice. Eur. J. Neurosci. *40*, 3294–3301. https://doi.org/10.1111/ejn.12689.

Sun, Y., Ikrar, T., Davis, M.F., Gong, N., Zheng, X., Luo, Z.D., Lai, C., Mei, L., Holmes, T.C., Gandhi, S.P., and Xu, X. (2016). Neuregulin-1/ErbB4 signaling regulates visual cortical plasticity. Neuron *92*, 160–173. https://doi.org/10.1016/j.neuron.2016.08.033.

Suttkus, A., Rohn, S., Jager, C., Arendt, T., and Morawski, M. (2012). Neuroprotection against iron-induced cell death by perineuronal nets - an in vivo analysis of oxidative stress. Am. J. Neurodegener. Dis. *1*, 122–129.

Verret, L., Krezymon, A., Halley, H., Trouche, S., Zerwas, M., Lazouret, M., Lassalle, J.M., and Rampon, C. (2013). Transient enriched housing before amyloidosis onset sustains cognitive improvement in Tg2576 mice. Neurobiol. Aging *34*, 211–225. https://doi.org/10.1016/j.neurobiolaging.2012.05.013.

Verret, L., Mann, E.O., Hang, G.B., Barth, A.M., Cobos, I., Ho, K., Devidze, N., Masliah, E., Kreitzer, A.C., Mody, I., et al. (2012). Inhibitory interneuron deficit links altered network activity and cognitive dysfunction in Alzheimer model. Cell *149*, 708–721. https://doi.org/10.1016/j.cell.2012.02.046.

Yamada, J., Ohgomori, T., and Jinno, S. (2015). Perineuronal nets affect parvalbumin expression in GABAergic neurons of the mouse hippocampus. Eur. J. Neurosci. *41*, 368–378. https://doi.org/10.1111/ejn.12792.

Yang, M., and Crawley, J.N. (2009). Simple behavioral assessment of mouse olfaction. Curr. Protoc. Neurosci. *Chapter 8*, Unit 8 24. https://doi.org/10.1002/0471142301.ns0824s48.

STAR★METHODS

KEY RESOURCES TABLE

REAGENT or RESOURCE	SOURCE	IDENTIFIER
Antibodies		
Wisteria Floribunda Agglutinin (WFA)- biotinylated	Sigma-Aldrich	Cat# L-1516, RRID:AB_2620171
Goat polyclonal anti-parvalbumin antibody	Swant	Cat# PVG213, RRID:AB_2721207
Rabbit polyclonal anti-purkinje cell protein 4 (PCP4)	Santa Cruz	Cat# sc-74816, RRID:AB_2236566
DyLight 549 Streptavidin antibody	Vector lab	Cat# SA-5549, RRID:AB_2336408
Donkey anti-Goat IgG (H + L) Cross-Adsorbed Secondary Antibody, Alexa Fluor 488	ThermoFisher Scientific	Cat# A-11055, RRID:AB_2534102
Donkey anti-Rabbit IgG (H + L) Highly Cross-Adsorbed Secondary Antibody, Alexa Fluor 647	ThermoFisher Scientific	Cat# A-31573, RRID:AB_2536183
Chemicals, peptides, and recombinant proteins		
Chondroitinase ABC	Sigma-Aldrich	Cat# C3667
Human Hereguline 1b	Peprotech	100-03
NBQX	TOCRIS	Cat#1431/1mg
D-AP5	Hello bio	HB0225-100mg
Experimental models: Organisms/strains		
Tg(APPSWE)2576Kha	Gift from Karen Hsiao	Cat# 3029285, RRID:MGI:3029285
C57BL/6J *Mus musculus*	Jackson lab	Cat# JAX:000664, RRID:IMSR_JAX:000664
Software and algorithms		
ImageJ- Used for image analyzing and quantification of intensity	ImageJ	https://imagej.net/Welcome
Mercator – Used for cell counting and stereology	Explora Nova	N/A
Axograph X software for data acquisition	Axograph	https://axograph.com
pClamp10- data acquisition	Molecular devices	https://www.moleculardevices.com
Origin Pro- data analysis	Origin Lab	https://www.originlab.com
GraphPad Prism version 6.00 and 9.00	GraphPad Software	https://www.graphpad.com

RESOURCE AVAILABILITY

Lead contact

Further information and requests for resources and reagents should be directed to and will be fulfilled by the lead contact, Laure Verret (laure.verret@univ-tlse3.fr).

Materials availability

This study did not generate new unique reagents.

Data and code availability

- All data reported in this paper will be shared by the lead contact upon request.
- This paper does not report original code.
- Any additional information required to reanalyze the data reported in this paper is available from the lead contact upon request.

EXPERIMENTAL MODEL AND SUBJECT DETAILS

Experiments were performed on female mice, aged from 9 to 10 months old, of the transgenic line Tg2576 (Hsiao et al., 1996) from our in-house colony. Tg2576 mice overexpress a double mutant form of human APP695 (Lys670-Asn, Met671-Leu [K670N, M671L]), driven by hamster prion protein promoter. Hemizygous Tg2576 males are bred with C57B6/SJL F1 females (Charles River, France). Mice are maintained 2 to 5 per

cage on a 12-hour light/12-hour dark cycle with free access to food and water. Littermates were randomly assigned to experimental groups. ChABC injections were performed on female C57BL/6J wild-type mice (WT; Charles River, France), aged from 4 to 6 months old. All experiments were performed in accordance with the policies of the European Union (2010/63/EU) for the care and use of laboratory animals. Our animal facility is fully accredited by the French Direction of Veterinary Services (D 31–555–11, Sep 19, 2016) and experimental procedures conducted in this study were authorized by local ethical committees and the French Ministry for Research (#20210–2019041014597476 v4, #02118.02, 2017, #12406-2016040417305913 v10).

METHOD DETAILS

Stereotaxic injections

Female from the Tg2576 line and C57BL/6J wild-type (WT) mice were anaesthetized with isoflurane before being submitted to two bilateral injections into dorsal hippocampal CA2 (coordinates relative to bregma for NTg and Tg2576 mice: –0.6 mm AP, ± 0.6 mm L and –2.05 mm DV, and –1.38 mm AP, ± 2.3 mm L and –2.00 mm DV; WT C57BL/6J: –1.1 mm AP, ± 0.6 mm L and –2.05 mm DV; and –1.98 mm AP, ± 2.3 mm L and –2.00 mm DV). 100 nL of a solution with ChABC (50 U/mL, Sigma, n = 12 mice), or of vehicle solution (phosphate buffer saline 0.1 M, PBS, n = 10 mice) were injected in female WT C57BL/6J mice. For NTg and Tg2576 mice, 100 nL of a solution with NRG1 (6.66 nM, n = 46 mice), or of vehicle solution (phosphate buffer saline 0.1 M, PBS, n = 41 mice) were injected in area CA2. The animals were then allowed to recover for 5 or 7 days before behavioral testing.

Behavioral experiments

Sociability and social recognition tests. Mice were placed in the center of a three-chamber setup (Moy et al., 2004), and were free to explore for 10 min. To assess sociability, the mice were placed in the presence of a littermate (familiar) mouse confined in a small cylindrical cage with bars, and an empty cage. Social recognition testing consisted of presenting a cage with a littermate (familiar) mouse, and another with an unfamiliar (new) mouse, never encountered before. The investigation time for each cage was measured using the Ethovision software (Noldus).

Five-trial social memory test. Mice were placed for 10 min in a 48 × 37 × 21 cm arena containing a small cage with bars (Kogan et al., 2000). An unfamiliar mouse (same age and sex) was introduced in the cage for four successive trials of 5 min (10 min inter-trial interval). On the fifth trial, a different unfamiliar mouse was presented. Mice were sacrificed 3 hours after the social memory test.

Object location test. During the acquisition, two identical objects were placed in the middle of a cylindric arena (40 cm diameter) containing a visual cue (striped pattern). The mice could freely explore the environment for 10 min. Three hours later, one object was moved, and the mice were allowed to explore for another 10 min.

Olfactory habituation/dishabituation test. Mice were placed in a cage with a perforated lid in the center of which cotton swabs soaked with non-social odors (almond and banana) and social odors (from two different cages of unfamiliar mice) were successively placed. Each odor was presented three times during two minutes.

Tissue preparation and immunohistochemistry

Mice were deeply anesthetized with dolethal and perfused transcardially with saline. Brains were post-fixed in 4% paraformaldehyde (two days at 4°C), then submerged in 30% sucrose solution. 30-µm-thick sections were cut on a sliding microtome (Leica SM2010R) equipped with a freezing-stage (Physitemp BFS-3MP), and placed in PB 0.1 M with saline and 0.25%Triton-X (PBST). Sections were then incubated in biotin-conjugated *Wisteria floribunda* agglutinin (WFA) lectin (1:1,000; Sigma, L1516), rabbit anti-PCP4 (1:500; Santa Cruz, sc-74816) and goat anti-PV antibodies (1:2,500; Swant, PVG213). The next day, floating sections were incubated for 90 min in a PBST solution containing 10% normal donkey serum, with 1:500 DyLight 549-streptavidin (Vector, SA-5549) for PNN, 1:250 donkey anti-goat A488 (ThermoFischer, A-11055) for PV, and 1:250 donkey anti-rabbit A647 (ThermoFischer, A-31573) for PCP4.

Image analysis

Quantification of PV+ and PV+/PNN + cells. Quantification of PV-immunoreactive (PV+) cells, and PV+ cells with PNN (PV+/PNN+) was conducted from a 1-in-10 series of sections spaced at 300 μm spanning the dorsal hippocampus (starting at -1.10 mm from bregma). For each mouse, quantifications of PV+, PNN+ and PV+/PNN+ cells were assessed manually with a fluorescence microscope (Leica DM6000 B) using controlled camera settings as previously described (Cattaud et al., 2018). The double labeling for PV and PNN was determined when WFA staining was entirely enveloping the soma of a PV+ cell, even if the staining was low. Changes of focal point were used to erase uncertainty. The corresponding surface of area CA2 and its different layers were defined with PCP4 staining and measured using the Mercator stereology system (Explora Nova). The total number of PV+ and PV+/PNN+ cells was estimated by multiplying the reference volume of area CA2 by the density of neurons by sectional volume (Canning et al., 1993; Cattaud et al., 2018).

Quantification of WFA intensity in whole CA1, CA2 and CA3 areas. Images were acquired on two sections per animal for CA2 and CA3 (–1.10 and –2.00 mm from bregma), and one section for area CA1 (–2.00 mm from bregma). Stratum oriens (SO), pyramidale (SP), and radiatum (SR) were delimited (ImageJ), and the mean grey value in each zone was measured. All images were analyzed as previously described (Domínguez et al., 2019), with the same methods of quantification by an experimenter blind to group and genotype: identification of the areas, delimitation of the layers, and extraction of the mean intensity of WFA fluorescence using the same parameters for all layers. These intensity values were normalized with WFA fluorescence intensity taken from the fimbria from the same sections in order to minimized variability due to difference of background.

Quantification of PV intensity in PV+ cells of CA2 area. To determine the intensity of PV fluorescence in the soma of PV+ cells, all the PV+ cells were picked in images from the SP of area CA2 from 2 sections stained for PV and PCP4 (–1.10 and –2.00 mm from bregma). The outline of the PV+/PCP4– soma was delimited with the free hand tool (ImageJ), and the mean grey value in each neuron was measured. These PV fluorescence intensity values were normalized with the average of PV fluorescence intensity taken from 4 PV–/PCP4+ cells from the same sections in order to minimized variability due to difference of background.

Electrophysiological recordings

Animals (9-12 months old) were heavily anesthetized with ketamine/xylazine and isofluorane and transcardially perfused with dissection solution containing (in mM): 93 NMDG, 2.5 KCl, 1.25 NaH_2PO_4, 30 $NaHCO_3$, 20 HEPES, 25 Glucose, 2 thiourea, 5 NaAscorbate, 3 Na-pyruvate, 0.5 $CaCl_2$, 10 $MgCl_2$, 93 HCl. Hippocampi were removed and placed into an agar mould and 400 μm transverse hippocampal slices were cut with a vibratome (Leica VT1200S, Germany) in ice-cold dissection solution. The slices were transferred to 30°C artificial cerebral spinal fluid (ACSF), (in mM: 125 NaCl, 2.5 KCl, 10 glucose, 26 $NaHCO_3$, 1.25 NaH_2PO_4, 2 Na Pyruvate, 2 $CaCl_2$ and 1 $MgCl_2$) for 30 min, and kept at room temperature for at least 1.5 hr before recording. All experiments were performed at 33°C.

Whole-cell recordings were obtained from CA2 pyramidal neurons in voltage- or current-clamp mode with a patch pipette (3–5 MΩ) containing (in mM): 135 K- or Cs-methyl sulfonate, 5 KCl, 0.1 EGTA-Na, 10 HEPES, 2 NaCl, 5 ATP, 0.4 GTP, 10 phosphocreatine; pH 7.2; 280–290 mOsm). Series resistance (12–18 MΩ) was monitored throughout each experiment and cells with more than 15% change were excluded from analysis. Before beginning whole cell experiments, the cell type was confirmed by several electrophysiological properties as previously described (Chevaleyre and Siegelbaum, 2010). Synaptic responses were evoked by mono-polar stimulation with a patch pipette filled with ACSF and positioned in the middle of CA1 SR to evoke antidromic spikes of CA3 input to CA2. Field recordings of PSPs were performed in current clamp mode with a recording patch pipette containing 1M of NaCl and positioned in the middle of SR or SP in area CA2. Field recordings and whole cell recordings of PSP were performed without GABA receptor blockers.

IPSCs were recorded in presence of ionotropic glutamatergic receptor blockers (DAP-V and NBQX). The paired pulse ratio was measured by dividing the amplitude of the second IPSC by the amplitude of the first IPSC (interval 100ms). For LTD experiments, the amplitudes of the IPSCs were normalized to the baseline amplitude. AHFS (100 pulses at 100Hz repeated twice, 20 sec apart) was applied following stable baseline. The magnitude of plasticity was estimated by comparing averaged responses at 30-40 min after the

induction protocol with baseline-averaged responses from 0 to 10 min before the induction protocol. We used pClamp10 and Axograph software for data acquisition and analysis.

QUANTIFICATION AND STATISTICAL ANALYSIS

Statistical analyses were performed using Origin Pro and Prism 6 and 9. Null hypotheses were rejected at the 0.05 level, unless Bonferroni's correction for multiple comparisons was applied; null hypotheses were rejected at the 0.0166 level when three comparisons were made, and at the 0.0125 level when four comparisons were made.